

Provided for non-commercial research and education use.  
Not for reproduction, distribution or commercial use.



(This is a sample cover image for this issue. The actual cover is not yet available at this time.)

This article appeared in a journal published by Elsevier. The attached copy is furnished to the author for internal non-commercial research and education use, including for instruction at the authors institution and sharing with colleagues.

Other uses, including reproduction and distribution, or selling or licensing copies, or posting to personal, institutional or third party websites are prohibited.

In most cases authors are permitted to post their version of the article (e.g. in Word or Tex form) to their personal website or institutional repository. Authors requiring further information regarding Elsevier's archiving and manuscript policies are encouraged to visit:

<http://www.elsevier.com/copyright>

Contents lists available at [SciVerse ScienceDirect](http://www.sciencedirect.com)

# Fire Safety Journal

journal homepage: [www.elsevier.com/locate/firesaf](http://www.elsevier.com/locate/firesaf)

## Experimental study on the performance of a load-bearing steel stud gypsum board wall assembly exposed to a real fire

Seul-Hyun Park<sup>a,1</sup>, Samuel L. Manzello<sup>a,\*</sup>, Matthew F. Bundy<sup>a</sup>, Tensei Mizukami<sup>b</sup><sup>a</sup> Fire Research Division, Engineering Laboratory (EL), National Institute of Standards and Technology (NIST), Gaithersburg, MD 20899, USA<sup>b</sup> Tsukuba Building Research and Testing Laboratory (TBTL), The Center for Better Living, Tsukuba, Ibaraki, Japan

### ARTICLE INFO

#### Article history:

Received 25 August 2009

Received in revised form

24 August 2011

Accepted 1 September 2011

#### Keywords:

Compartment fire

Fire resistance

Load-bearing wall

### ABSTRACT

The National Institute of Standards and Technology (NIST) and the Center for Better Living (CBL) have formed an international collaboration to assess the performance and failure mechanisms of gypsum wall assemblies under real fires/furnace conditions. In an effort to compile an experimental database necessary to validate models that could be used to predict their performance and ultimate failure under various design fires, a full scale test was conducted in the Large Fire Laboratory (LFL) at NIST. This paper provides a valuable experimental data set on the performance of a full scale loaded gypsum steel stud assembly exposed to an intense full scale compartment fire.

Published by Elsevier Ltd.

### 1. Introduction

While standard fire resistance testing has reduced the number of fires that have resulted in loss of life, the inability of the fire resistance rating to act as an absolute predictor of performance in an actual fire was recognized from the beginning. Standard fire resistance tests are conducted under furnace conditions and furnace data is of limited use to validate computational models that could be used to predict the performance and failure of these assemblies under arbitrary fire loadings [1–3]. Specifically, realistic fires do not heat assemblies uniformly or in a continuous manner, and real fires move causing the assembly to cool even in the presence of smoke and flames.

There is no documented understanding of the performance and failure of load bearing steel stud gypsum board wall assemblies under realistic fire conditions; this greatly hampers the application of performance-based design approaches. Data and sub-model implementation in EL's Fire Dynamics Simulator (FDS) of gypsum assembly failure will enable performance based design and afford the ability to quantify how fire spreads from one compartment to another. Load bearing steel stud gypsum assemblies are an ideal construction assembly to investigate the failure mechanism of load bearing structure as these are very common.

Without physical knowledge of actual performance and failure mechanisms under realistic fires, it is impossible to predict the time of failure of a load bearing steel stud gypsum board wall assembly under fire exposures. Such information is critical to estimate safe egress times from buildings and provide guidance to firefighters entering a building. To this end, the National Institute of Standards and Technology (NIST) and the Center for Better Living (CBL) have formed an international collaboration to assess the performance and failure mechanisms of gypsum wall assemblies under real fires/furnace conditions and to compile an experimental database necessary to validate models that could be used to predict their performance and ultimate failure under various design fires.

In support of this collaboration, the first ever experiment to expose a full scale loaded gypsum steel stud assembly to an intense compartment fire was conducted as a proof-of-concept exercise in order to determine the feasibility of such testing. Results obtained from this experiment are presented and discussed.

### 2. Experimental description

The experiment was conducted in the Large Fire Laboratory (LFL) at NIST. A major focus of this work is to be able to compare the performance/failure of loaded assemblies under realistic fire exposures to that of furnace exposures. Accordingly, a wall was constructed using two layers of 15.9 mm thick type X gypsum board attached to a custom-built self-supporting steel stud frame. The specific dimensions of the steel stud frame assembly are

\* Corresponding author. Tel.: +1 301 975 6891; fax: +1 301 975 4052.

E-mail address: [samuelm@nist.gov](mailto:samuelm@nist.gov) (S.L. Manzello).

<sup>1</sup> Space Application & Future Technology Center, Korea Aerospace Research Institute (KARI), Deajeon 305-333, South Korea.

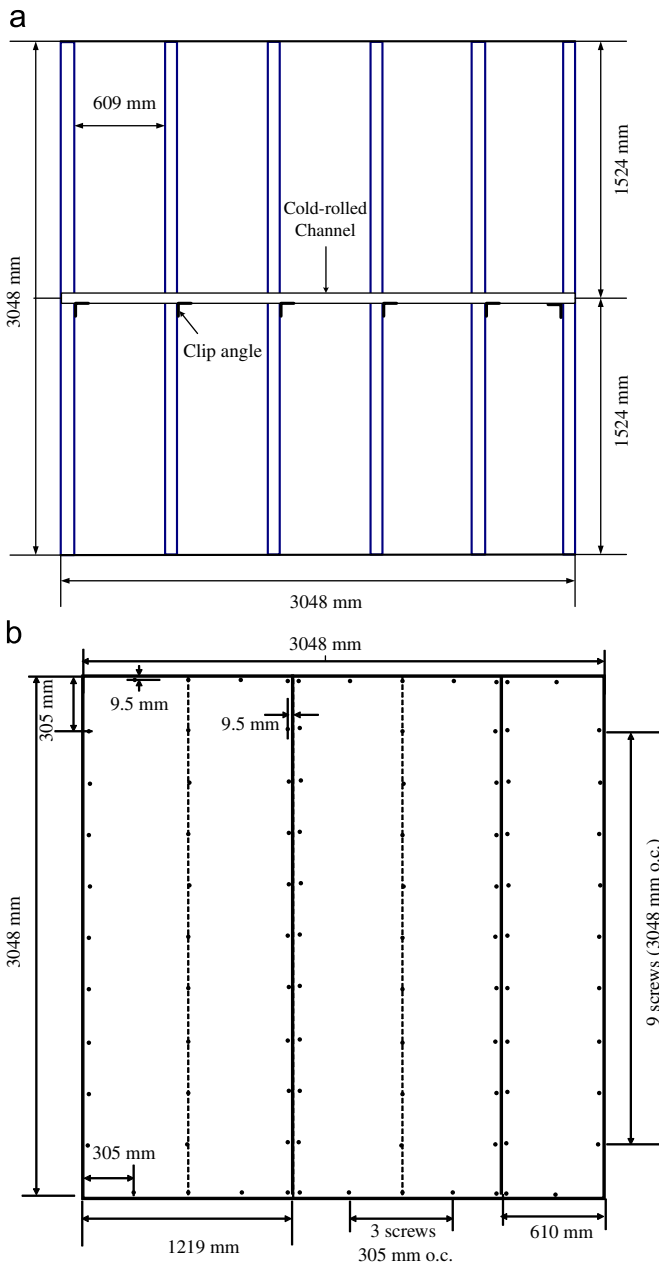


Fig. 1. Schematic of load-bearing steel stud/gypsum wall assembly: (a) steel frame assembly; and (b) gypsum wall assembly attached to studs.

shown in Fig. 1a. Steel studs with yield strength of 228 MPa were equally spaced at 609 mm, and a bridging channel (3.0 m long) was installed at mid-height of the frame. The installation of the gypsum board to the studs was performed in accordance with ASTM guidelines [4–7]. Fig. 1b displays the steel stud gypsum wall assembly that includes two layers of gypsum board on each face. Each layer consisted of three single gypsum board panels; two with dimension of 1219 mm × 3048 mm and one gypsum board panel with dimensions of 610 mm × 3048 mm. Each was attached to the studs using type S drywall screws. The seams of each layer were then staggered as done in practice.

To quantitatively investigate the performance/failure of loaded assemblies exposed to the real fire, temperatures were measured using type K thermocouples (22 gage) installed at various locations of the steel stud gypsum wall assembly. The locations included (1) inside the interior cavity of the assembly (twenty thermocouples), and (2) the unexposed surface (nine thermocouples). Detailed

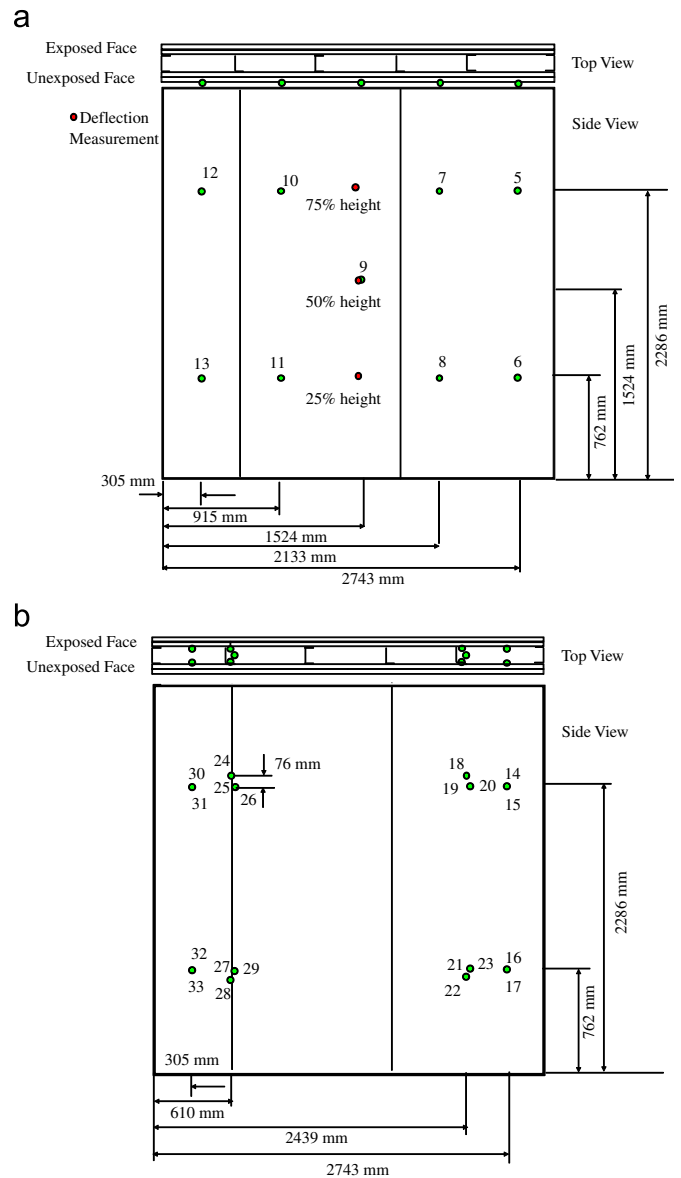
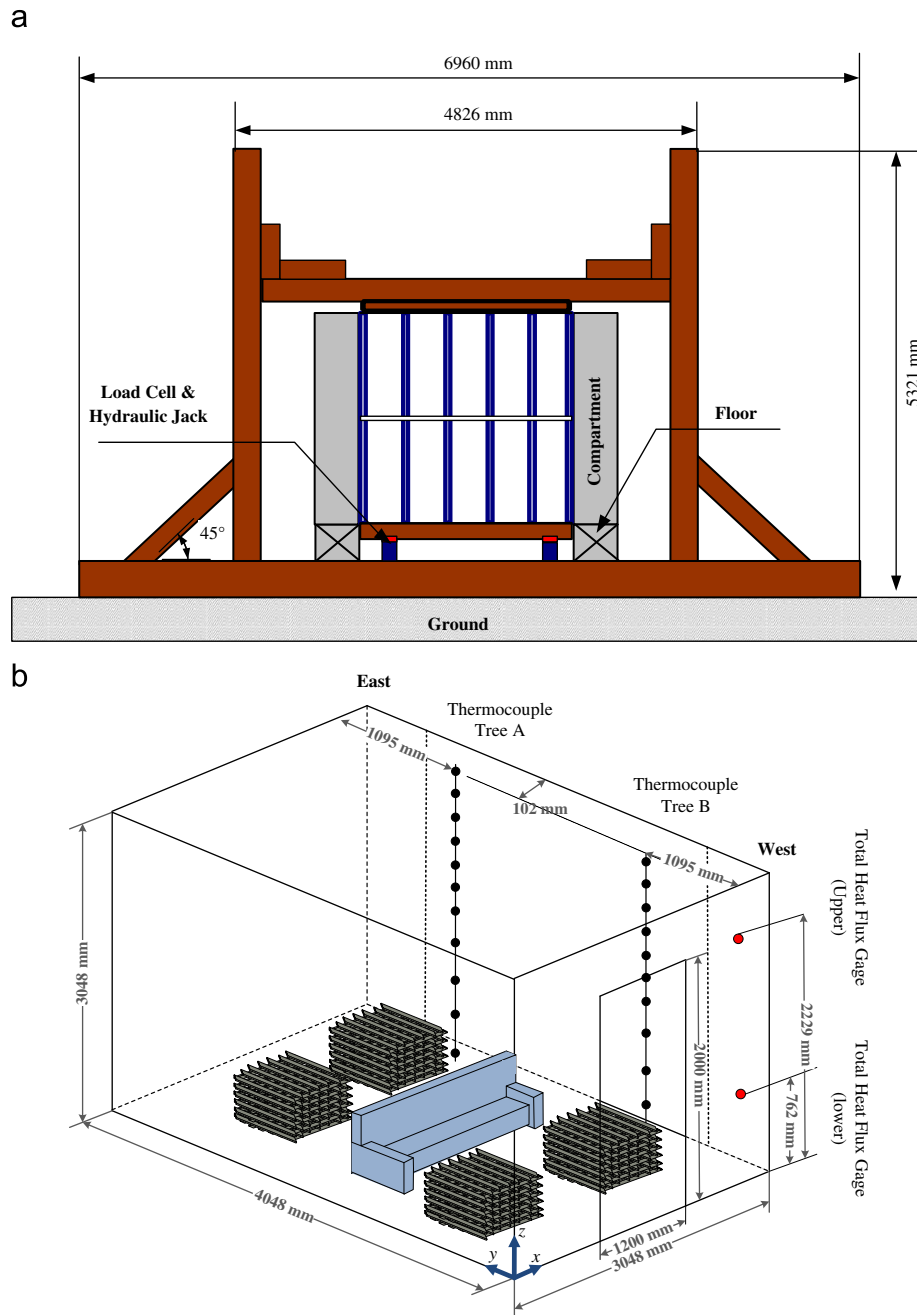


Fig. 2. Drawing of the test wall assembly showing the location of thermocouples and deflection gages installed: (a) location of thermocouples and deflection gages on the unexposed face; and (b) location of thermocouples inside the cavity.

information on the locations of the thermocouples is displayed in Fig. 2a and b.

A robust steel loading frame was first set to the test position and the test wall assembly was then positioned in between the loading beam (sitting on two hydraulic jacks) and an upper beam (fitted to the top of the test assembly). In order to prevent the test wall assembly from falling out (in the event that test wall assembly failed), the top and bottom tracks of the test wall assembly (only the track) were screwed, respectively, to top and bottom beams.

A compartment of dimensions 3048 mm (width) × 3048 mm (height) × 4048 mm (length) was finally placed against the loading frame (see Fig. 3a–b). Gaps between the compartment and the test wall assembly were sealed with fire-resistant ceramic fiber material. The compartment was designed not to interact mechanically with the test wall assembly. This design is very similar to how the thermal exposure is provided during furnace testing [1,8]. A 1200 mm × 2000 mm opening was constructed at the western side of the compartment. As shown in Fig. 3a, the



**Fig. 3.** Schematic of test facilities and the compartment: (a) front view of the compartment equipped with a gypsum stud wall assembly and test facilities; and (b) perspective view of the compartment.

steel stud gypsum wall assembly was loaded via two hydraulic jacks mounted on the bottom of the test frame. A load cell was mounted above each of the hydraulic jacks. Each of the load cells was calibrated using instrumentation in the NIST manufacturing metrology division prior to the test. In these calibration tests, various loads were applied to the load cells and a plot of voltage as a function of applied load was generated. The applied loads during the calibration procedure encompassed the full range of load detectable with these particular load cells. In this study, the applied load to the test wall assembly was a nominal value of 65 kN, which corresponded to 90.5% of the maximum design load. The maximum design load was determined by following the specification of the design of a cold-formed steel structural member proposed by the American Iron and Steel Institute (AISI) [9].

During the test, horizontal deflection at three points (25% wall height, 50% wall height, and 75% wall height; (see Fig. 2b) was also measured on the test wall assembly in order to examine the out-of-plane deflection of the assembly. In addition, the vertical displacement of the sliding platen that rested on the hydraulic jacks was measured.

The combustibles within the compartment consisted of four wood cribs (50 kg each) and one sofa (polyurethane foam supplemented with wood, 45 kg, 1750 mm in length  $\times$  950 mm in depth  $\times$  750 mm in width). This combination of combustibles has been used to accelerate initial fire growth in prior compartment tests focused at determining performance/failure of non-load bearing gypsum assemblies under realistic fires [10]. The fire was initiated by igniting the sofa. Measurements inside the compartment consisted of two thermocouple trees to measure

temperature and two total heat flux gages mounted near the loaded test wall to quantify heat flux that the test wall received. A thermocouple tree was located near the doorway (approximately 1.1 m away from the western side of compartment wall) and near the corner opposite the doorway (approximately 1.1 m away from the eastern side of compartment wall). Each tree included ten thermocouples, which were located nominally 300 mm apart with the highest thermocouple positioned 50 mm below the ceiling. The total heat flux gauges were water cooled to  $60 \pm 5$  °C in order to mitigate water condensation on the surface of gauges during the test. The total heat flux gauges used were calibrated at NIST prior to the test at the water cooling temperature.

The exhaust of the compartment was directed to the 9.0 m × 12.0 m large scale exhaust hood and calorimeter to determine the heat release rate using oxygen consumption calorimetry [11]. The compartment design and fuel loading was based on the work of Jones [12]. Since this test was a proof-of-concept exercise, the fuel load used was reduced as compared to Jones [12] to limit the duration of the fire in order to verify the performance of the frame (and concept) constructed for these experiments.

### 3. Results and discussion

Fig. 4 displays temporal images of the compartment fire development after ignition. Piloted ignition initiated on the sofa resulted in a rapidly developing fire. As shown in the figure, the onset of flashover was observed approximately 260 s after ignition and then a ventilation-controlled fire developed. As the fuel was consumed, the fire began to diminish 1080 s after ignition. The maximum radiant intensities (judged by the luminosity from fire) in the compartment were observed around 1300 s after ignition (See Fig. 4).

Fig. 5 displays the measured heat release rate (HRR) as a function of time. In the figure, the measured HRR rapidly increased over a period of approximately 260 s, producing the first peak of HRR, which occurred at the onset of flashover. During this period, radiant heat from the fire resulted in ignition of two cribs located at the western side of the compartment, accelerating the transition to a fully developed fire. As the fire grew into the fully developed phase, two identical peaks of HRR of 3710 kW were observed. This can be attributed to the fact that the fuel (i.e., pyrolysates from cribs and a sofa) in the western side of the compartment was consumed faster than that in the eastern side. This interesting phenomenon can be confirmed by gas-phase temperatures measured from each thermocouple tree installed at different locations of the compartment (which are displayed and discussed in Fig. 6).

Fig. 6a–b displays the measured temperatures inside the compartment as a function of time after ignition. In Fig. 6b, two distinct peaks (except for bottom regime) were observed in

temperature measured from the thermocouple tree B (installed close to the door way), similar to the HRR measurement. After flashover, more radiant energy was delivered to the cribs installed near the door way (compared to those inside the compartment) due to the projected flames, resulting in fast fuel pyrolysis reactions and thus the first peak of the HRR. As a result, the rate of temperature rise measured from thermocouple tree B was much faster than that measured from thermocouple tree A over the same period (between 600 s and 900 s). This result suggests that the fuel load distribution will affect the temperature profiles inside the compartment. Therefore, the thermal loads that are delivered to the structure exposed to real fires will not be uniform along the compartment in contrast to the furnace exposure tests. As temperatures inside the compartment rapidly increased, fuel produced from the cribs installed at the rear of the compartment began to burn actively, producing the second peak of the HRR.

In Fig. 6a–b, the time–temperature histories specified in ASTM E119 testing protocol [13] and parametric fire equations (given in Annex A of Eurocode 1 [14]) were also plotted for a direct comparison to that of real fire exposure in this experiment. These prescribed time–temperature curves have been commonly used for a standard fire resistance testing of load bearing steel stud gypsum board wall assemblies [1,8,15]. The time–temperature relationship prescribed by ASTM E 119 in Fig. 6 was fitted using

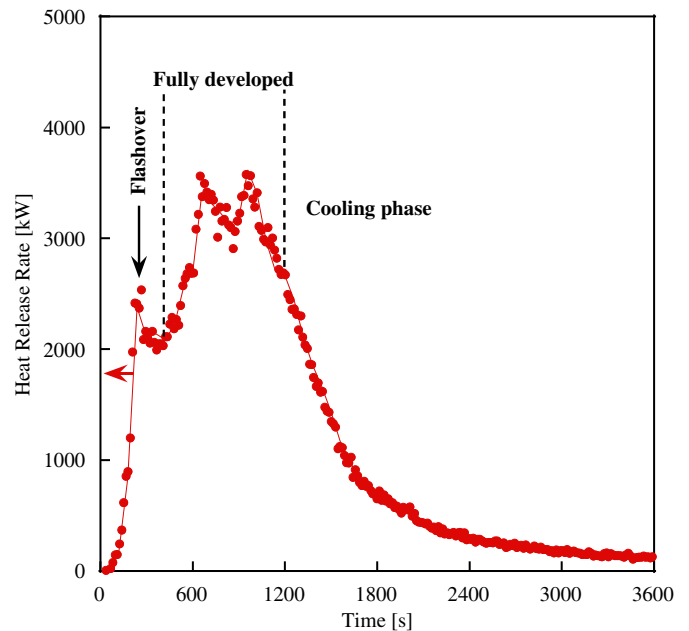


Fig. 5. Measured heat release rate and total heat fluxes as a function of time.

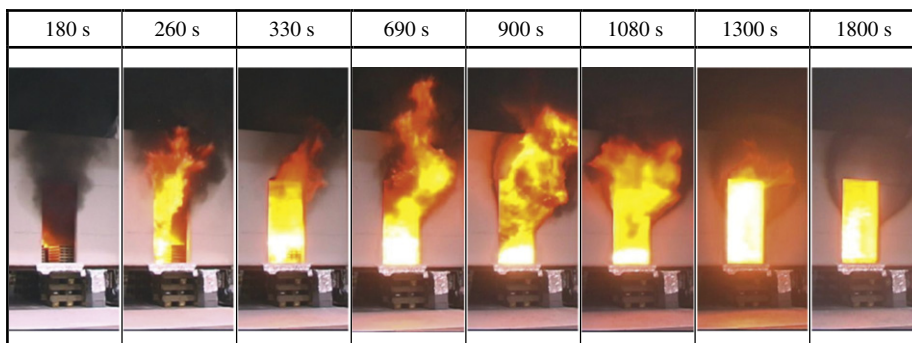


Fig. 4. Sequential images of compartment fire after ignition.

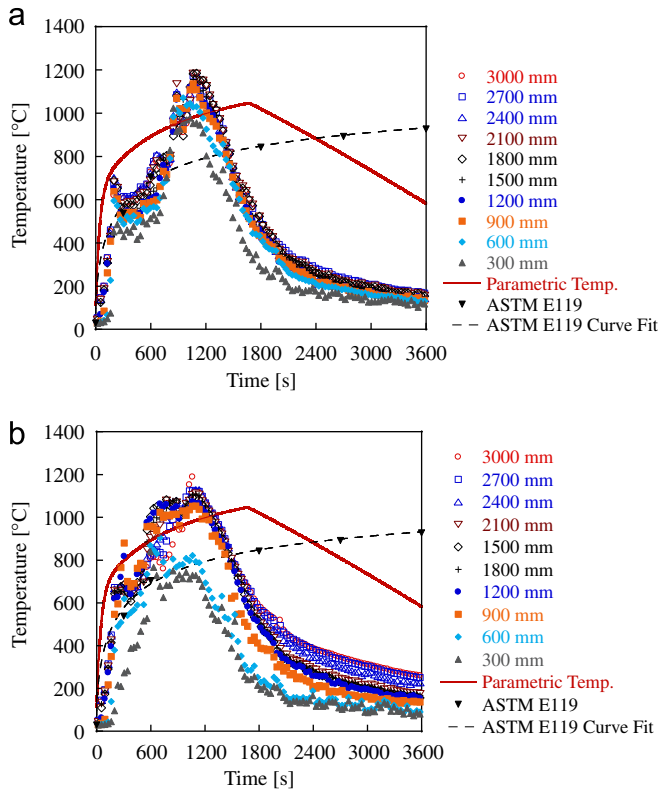


Fig. 6. Measured temperatures as a function of time: (a) eastern side of compartment; and (b) western side of compartment.

the following equation [16]:

$$T = 750[1 - \exp(-0.49\sqrt{t})] + 22\sqrt{t} + T_a \quad (1)$$

where  $T$  is the temperature,  $t$  is the time (in minutes), and  $T_a$  is the ambient temperature. In the figure, the parametric fire temperature curve for the heating phase of the fire was calculated using the following relationship [14]:

$$T = 20 + 1325[1 - 0.324\exp(-0.2t^*) - 0.204\exp(-1.7t^*) - 0.472\exp(-19t^*)] \quad (2)$$

where  $t^*$  is the fictitious time defined as  $t \cdot T$  (in hour),  $T$  is given as  $(F_v/0.04)^2/(b/1160)$ ,  $F_v$  is the opening factor, and  $b$  ( $=700 \text{ J/m}^2 \text{ s}^{1/2} \text{ K}$  [15]) is the thermal inertia of the bounding materials of the fire compartment. More details on variables and cooling phase time–temperature calculation are well summarized elsewhere [14].

Except for the bottom regime of the western side of the compartment, the measured temperatures from real fire exposures increased in a rate similar to other time–temperature curves until flashover. After this period, the rate of temperature rise measured from each thermocouple tree was much faster and greater than that observed in other time–temperature curves. The measured temperatures in the compartment continued to increase until 1200 s, reaching a maximum temperature of 1200 °C, and then decayed. In contrast to the ASTM E 119 time–temperature curve (that continuously increased and does not decay), the parametric fire temperature curve produced a fair approximation in terms of estimating the maximum compartment temperature and its corresponding time (although the maximum compartment temperature is slightly lower and its corresponding time is overestimated compared to real fire measurements). However, there was a large difference in the temperature decay rate between the two cases for the cooling phase. In addition, the parametric fire temperature curve does not

take the influence of fuel distribution (that resulted in two different peaks in the temperature and HRR) into consideration.

The total heat flux impinging on the surface of the compartment wall was measured using two heat flux gauges (vertically mounted 762 mm and 2229 mm away from the compartment floor) and is displayed in Fig. 7. It is important to note that the total heat flux gauges were not installed on the test wall assembly to protect them from possible damage caused by structural failure and, more importantly, not perturb the test wall itself. For comparison, the total heat flux measured in a furnace test operated following the ASTM E119 testing protocol [17] was also plotted in the figure. Initially, heat fluxes measured from both the real fire and furnace exposures were similar, suggesting that the ASTM E119 method produces a similar magnitude of thermal load as the real fire test performed in this particular study. After the onset of flashover (approximately at 260 s), the total heat flux measured for the real fire exposures, however, increased much faster compared to that for the furnace exposures, reaching the maximum value for both locations approximately at 1300 s. The measured heat flux distributions in the present study were very similar to those measured from other real fire tests [18,19]. Another significant difference in the measured total heat flux, compared to the furnace exposures, was that the magnitude of the total heat flux varied as a function of height in the compartment. For furnace exposures, the measured total heat was of the same magnitude, irrespective of height of the furnace. For the load-bearing wall assembly subjected to non-uniform heat flux distributions along the height, a thermally induced curvature (due to thermal load) can affect the integrity of structural elements and thus some elements can attain the load limit, causing the structural failure [20].

In order to investigate the influence of the fire's thermal load on the integrity of structural elements, the cumulative radiant energy,  $E$ , impinging on the surface of the test wall assembly was calculated using the following relationship [15]:

$$E = \varepsilon\sigma \int_0^t T^4 dt \quad (3)$$

where  $\varepsilon$  is the emissivity of the gas (assumed to be equal to 1) and  $\sigma$  is the Stefan–Boltzmann constant. This method assumes that

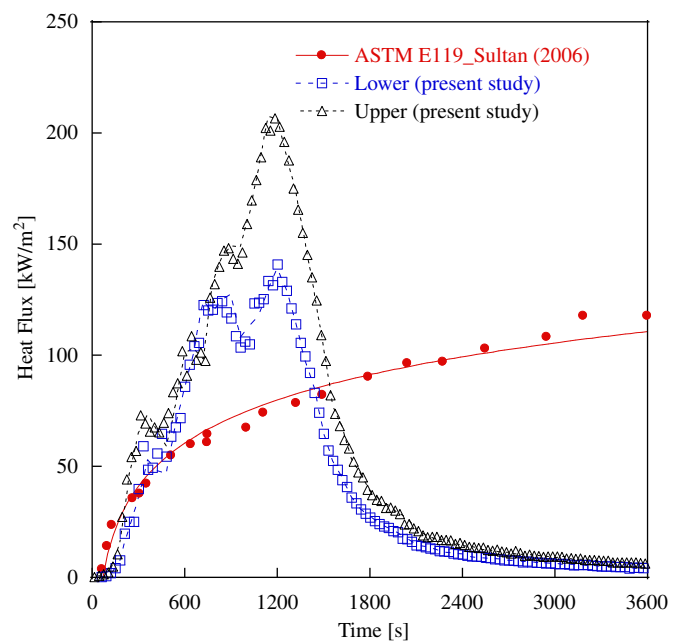


Fig. 7. Total heat flux comparison between real fire exposure and furnace tests.

the contribution of convective heat transfer to the test wall assembly is negligible since most of the energy transferred to the test wall assembly is strongly affected by radiative heat transfer (that is coupled with the fourth power of the gas temperature).

The cumulative radiant energy,  $E$ , was calculated using the averaged compartment fire temperature along the height (determined from temperature profiles in Fig. 6a–b) and plotted against time in Fig. 8a–b. For comparison, the calculated  $E$  from the ASTM E119 time–temperature curve (i.e., furnace exposures) was also plotted in the figure. The calculated  $E$  for the furnace exposures continuously increased; for the real fire exposure in the present study it was clearly divided into three phases. In phase I, the calculated  $E$  for both in real fire and furnace exposures slowly increased, keeping a similar value in magnitude, suggesting that the ASTM E119 method produced a similar magnitude of thermal load with the real fire test performed in this particular study during this phase. In phase II, there were distinct deviations in  $E$

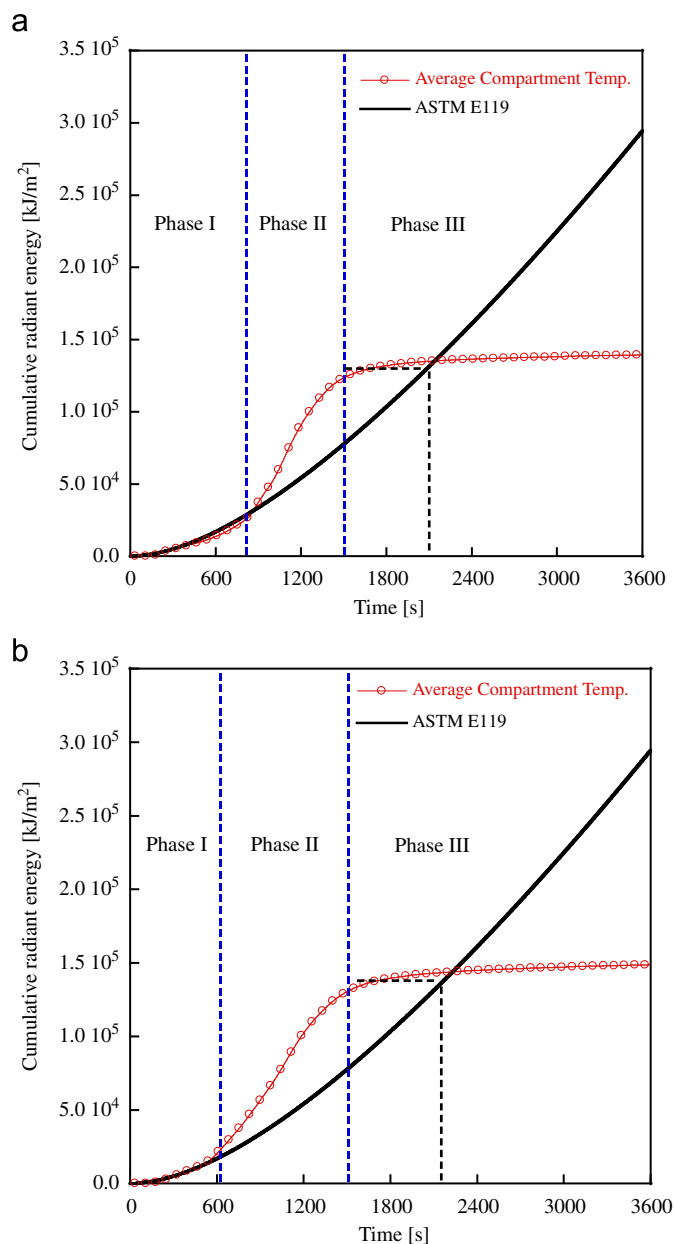


Fig. 8. Calculated cumulative radiant as a function of time: (a) eastern side of compartment; and (b) western side of compartment.

for each of the exposures. The rate of  $E$  rise for the real fire exposures was much faster compared to that for the furnace exposures expected for the bottom regime of the compartment. In Fig. 8a, for example, the time at which the test wall assembly is exposed to  $1.3 \times 10^5$  kJ/m<sup>2</sup> was approximately 1500 s (near the end of phase I) for the real fire exposures while the equivalent magnitude of  $E$  for the furnace exposures was observed approximately at 2250 s. Similar behaviors were observed in Fig. 8b. It is also interesting to note that a maximum value in the calculated  $E$  is higher in the western side of the compartment than in the eastern side but the transition of  $E$  from phase II to phase III at both locations occurs at the same time ( $t=1500$  s). For the real fire exposure test performed in this study, the steel studs installed near the door way, therefore, would be subjected to most severe thermal load.

The performance of the test wall assembly in this experiment was considered relative to the failure criteria delineated in ASTM E119. Based on the guidelines dictated in ASTM E119, the load-bearing test wall assembly was considered to have failed if any of the following was observed: (1) the temperature rose to more than 180 °C (above the ambient temperature) at a single point measurement on the unexposed face or the average temperature rise on the unexposed face was greater than 140 °C, (2) the passage of hot gases or flame through the assembly occurred, and (3) the assembly was observed to lose its ability to sustain the applied load. For criteria 1 and 2, the temperature of the unexposed face of the test wall assembly was measured by thermocouples installed at designated locations and an infrared camera was used to image the entire surface of unexposed face. For the last criterion, lateral and vertical deflection was measured to inspect the structural deformation (See Fig. 2b) and the test wall assembly was imaged from two different angles using a standard video camera.

Measured interior temperatures are displayed in Fig. 9a: those temperatures measured on the inside of the exposed face of the assembly. Fig. 9b displays temperatures measured on the inside of the unexposed face. The maximum temperature measured on the steel studs and gypsum board inside the cavity did not exceed 130 °C. In addition, the unexposed face temperatures measured on designated locations were found to be less than 60 °C (see Fig. 10). This was mainly due to the good thermal protection of two layer gypsum boards (2 h fire resistance rating) combined with the relatively short fire exposures, which allowed both gypsum board layers on the exposed face to remain intact and prevented them from falling out during the experiment. The reactions in which crystalline gypsum dehydrates and water is liberated occur between 125 °C and 225 °C and help establish the fire resistance properties of gypsum wall assembly [21,22]. In the previous load bearing tests performed in the furnace [1], severe cracks and fall off of gypsum board on the fire-exposed face occurred several minutes prior to structural failure, resulting in the overall out-of-plane bucking of the test wall assembly. Therefore, it was concluded that the number of the gypsum board layer as well as the fire-retarding properties of gypsum boards are a major factor contributing to the fire resistance characteristics of the load bearing gypsum steel stud wall assembly. Even though an opening at the joint between the two vertically mounted gypsum boards and traverse cracks were observed in this study, similar to previous non-load bearing tests in real fire exposure [2], they were limited to the face layer of the exposed side (see Fig. 11). This minimized the conduction through gypsum layers (on exposed side) to interior cavity of the test assembly. In addition, the temperature of the unexposed face was not observed to be greater than 60 °C; clearly failure based on the temperature rise criterion was not observed. Due to good thermal protection, any passage of flame or fire through the test wall assembly was

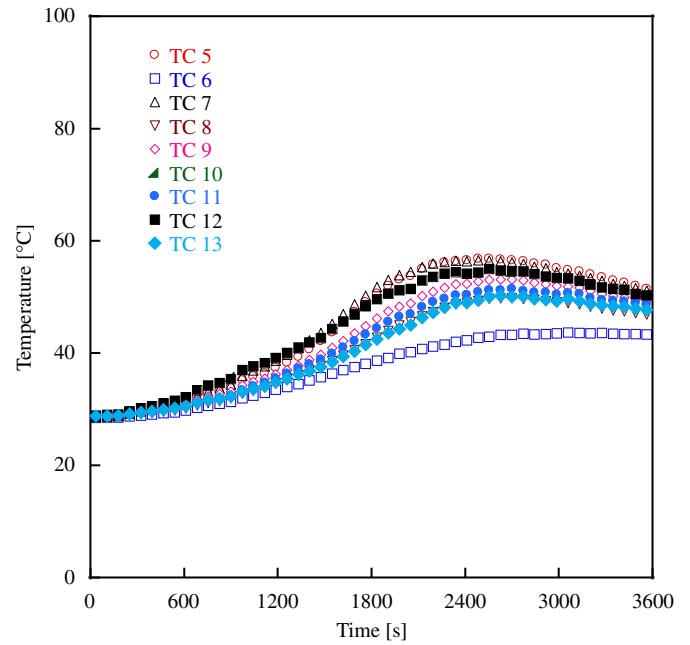
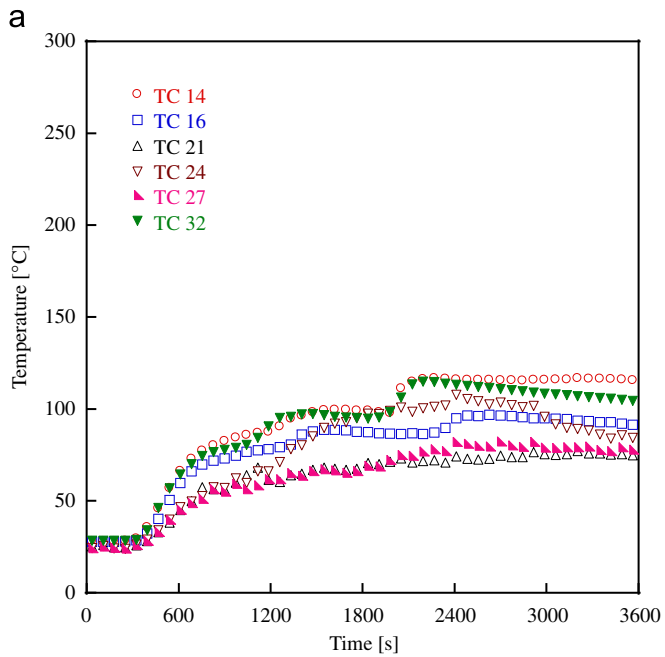


Fig. 10. Measured temperatures on the unexposed face.

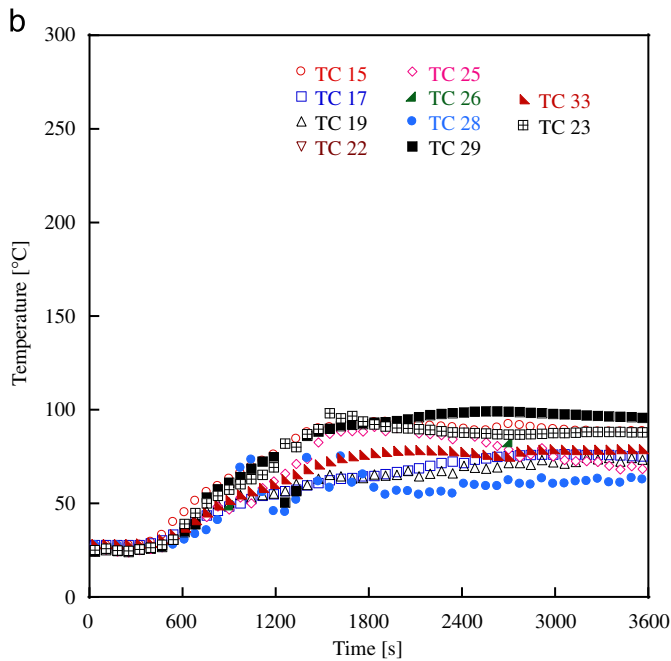


Fig. 9. Temperature profiles inside the interior cavity: (a) measured temperatures on the inside of the exposed face; and (b) measured temperatures on the inside of the unexposed face.



Fig. 11. Picture of the exposed face immediately after the extinguishment of the fire.

not observed from the IR measurements. Thus, the second ASTM E119 failure criterion was not satisfied.

As the fire became more intense, the test wall assembly subjected to the vertical load will degrade further and structural deformation may occur, which can result in the structural failure eventually described in criterion 3. To quantify the ability of the assembly to sustain the applied load, the horizontal deflection,  $\delta$  was measured using three deflection meters (potentiometers) along the height of the central part of the test wall assembly. Fig. 12a–b displays the measured  $\delta$  along the height of the central part of the test wall assembly (25% wall height, 50% wall height, and 75% wall height) and vertical displacement of the sliding platen measured at the western and eastern side of the compartment as a function of time. As shown in Fig. 12b, the vertical

displacement of the sliding platen was due to thermal expansion of the studs, similar to other studies [1,8].

The horizontal deflections represent the sum of stress-free thermal bowing due to a temperature gradient across the steel stud and secondary deflection due to the load applied to the steel studs [9]. In this study, the positive values of deflection measured are due to the movement of the test wall assembly inward in the direction of the compartment. The deflection caused by the applied load prior to ignition was offset in the present study. As the fire progressed, thermal bowing became dominant, producing a distinguished change in  $\delta$  approximately 1500 s after ignition for all heights investigated (see Fig. 12a). Interestingly, this time coincides well with the time when  $E$  reached the maximum value at the end of phase II. The maximum  $\delta$ , 10.7 mm was observed at

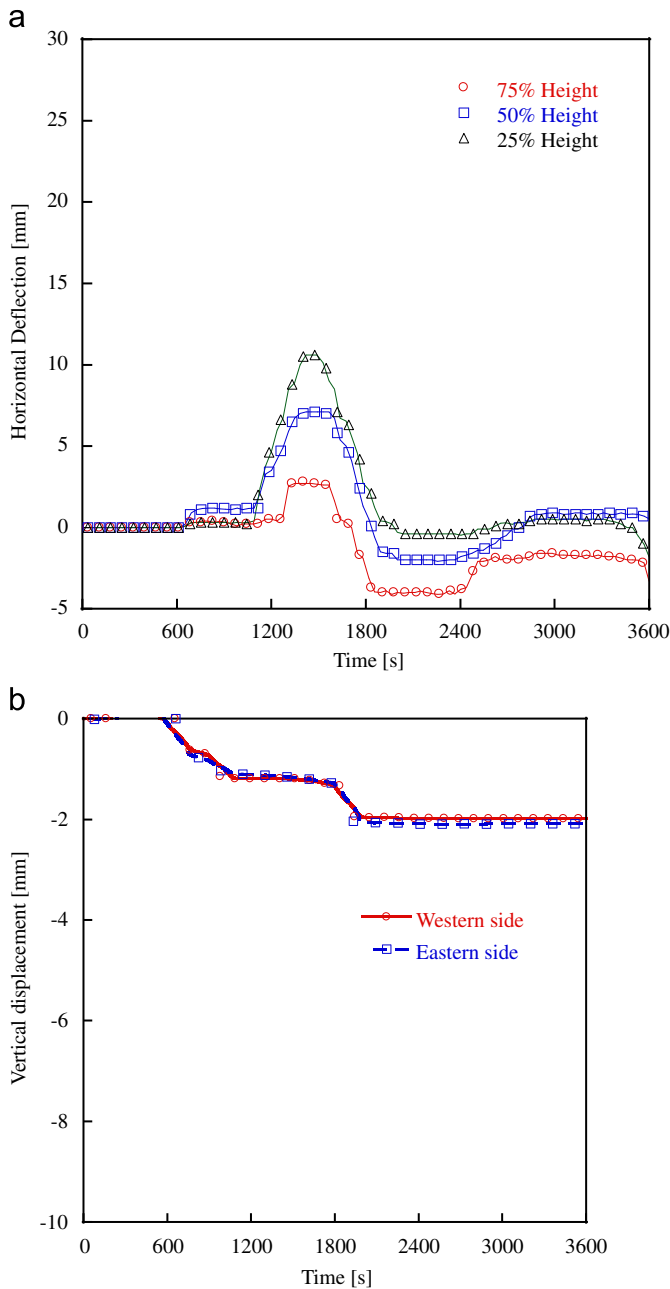


Fig. 12. Horizontal deflection and vertical displacement profiles plotted as a function of time: (a) horizontal deflection; and (b) vertical displacement.

25% wall height, followed by 7.1 mm at 50% wall height, and 2.7 mm at 75% wall height. Since the duration of the fire was limited by reduced fuel loads (manifested by HRR and heat flux measurements), the measured  $\delta$  immediately decreased as the fire diminished. It was also found that the observed variations in  $\delta$  did not cause the loss of ability of the test assembly to sustain the applied load.

A challenge with ASTM E119 is that failure to maintain the load is subjective. ISO 834, a similar international standard, has defined conditions for determining failure of loaded wall assemblies; similar failure criteria exist in ISO 834 for temperature rise on the unexposed face. For a loaded assembly, these are given as  $C > h/100$  (mm) and  $dC/dt > 3h/100$  (mm/min) (4)

where  $C$  is the axial contraction,  $h$  is the initial height of test wall assembly, and  $t$  is the time. In addition to the lateral deflection

reported above, the axial contraction caused by the upward movement of the loading beam (as the test wall bowed inward) was measured to further investigate the failure mechanism of the test wall assembly. For the present experiment, the ISO 834 failure criterion was not satisfied and therefore the test assembly did not fail under the ISO 834 condition as well. Although the test wall assembly did not fail under the real fire conditions in this experiment, based on ASTM E119 and ISO 834 methods, the experiment provides very valuable insight into how a load-bearing gypsum steel stud assembly performed under realistic fire exposures. For example, the deflection measured reached a maximum as the measured total heat flux for the real fire exposure test became significantly larger and then began to decrease with reductions in the heat flux applied on the wall. These experimental results clearly indicate the measured deflection was strongly dependent on the fire exposure conditions.

#### 4. Summary

In this study, the time–temperature histories specified in the ASTM E119 testing protocol and parametric fire equation in Annex A of Eurocode 1 were plotted for a direct comparison to that of real fire exposure in this experiment. In contrast to the ASTM E 119 time–temperature curve (that continuously increased and does not decay), the parametric fire temperature curve produced a fair approximation in terms of estimating the maximum compartment temperature and its corresponding time (although the maximum compartment temperature is slightly lower and its corresponding time is overestimated compared to real fire measurements). However, there was a large difference in the temperature decay rate between the two cases for the cooling phase. In addition, the parametric fire temperature curve does not take the influence of fuel distribution (that resulted in two different peaks in the temperature and HRR) into consideration. The measured deflection was strongly dependent on the total heat flux that varied with height for the real fire exposures. The measured heat flux distributions in the present study were very similar to those measured from other real fire tests [18,19].

To investigate the influence of the fire’s thermal load on the integrity of structural elements, the cumulative radiant energy,  $E$ , impinging on the surface of the test wall assembly was calculated and compared to the ASTM E119 furnace exposure. In phase I, the calculated  $E$  for both in real fire and furnace exposures slowly increased, keeping a similar value in magnitude, suggesting that the ASTM E119 method produced a similar magnitude of thermal load with the real fire test performed in this particular study during this phase. In phase II, there were distinct deviations in  $E$  for each of the exposures.

To quantify the ability of the assembly to sustain the applied load, the horizontal deflection,  $\delta$  was measured using three deflection meters (potentiometers) along the height of the central part of the test wall assembly. As the fire progressed, thermal bowing became dominant, producing a distinguished change in  $\delta$  approximately 1500 s after ignition for all heights investigated. Interestingly, this time coincides well with the time that  $E$  reached the maximum value at the end of phase II.

Although the load bearing test wall assembly did not fail for the fire load used in this experiment (maximum HRR of 3710 kW), it was shown that tests provided useful information on the performance of a loaded assembly under realistic fire. While additional full scale experiments under a variety of real exposures are required to fully elucidate failure mechanisms, the authors hope that this proof-of-concept exercise will motivate further study of not just gypsum wall assemblies under real fire exposures but other loaded structural members, including connections.

## Acknowledgments

The authors acknowledge the able assistant of the Large Fire Laboratory (LFL) staff. In particular, the help of Mr. Lauren DeLauter, Mr. Tony Chakalis, and Mrs. Doris Rinehart is greatly appreciated. Mr. Marco G. Fernandez, Engineering Technician of the Fire Measurements Group at EL-NIST was critical in conducting these tests. Dr. John Gross and Mr. Frank Davis of the Materials and Construction Research Division at EL-NIST provided indispensable guidance in assisting in the construction of the system used to provide the load to the test wall.

## References

- [1] V. Kodur, M. Sultan, Factors influencing fire resistance of load-bearing steel stud walls, *Fire Technol.* 42 (2006) 5–26.
- [2] S.L. Manzello, R.G. Gann, S.R. Kukuck, K. Prasad, W.W. Jones, Real fire performance of partition assemblies, *Fire Mater.* 29 (2005) 351–366.
- [3] S.L. Manzello, R.G. Gann, S.R. Kukuck, D.B. Lenhart, Influence of gypsum board type on real fire performance of partition assemblies, *Fire Mater.* 31 (2007) 425–442.
- [4] Standard Specification for Installation of Steel Framing Members to Screw-Attached Gypsum Panel Products, ASTM C754-00, American Society for Testing and Materials.
- [5] Standard Specification for Application of Finishing of Gypsum Board, ASTM C840-03, American Society for Testing and Materials.
- [6] Standard Specification for Nonstructural Steel Framing Members, ASTM C654-00, American Society for Testing and Materials.
- [7] Standard Specification for Steel-Piercing Tapping Screws for the Application of Gypsum Panel Products or Metal Plaster Bases to Wood or Steel Studs, ASTM C1002-01, American Society for Testing and Materials.
- [8] J.T. Gerlich, P.C.R. Collier, A.H. Buchanan, Design of light steel-framed walls for fire resistance, *Fire Mater.* 20 (1996) 79–96.
- [9] North American Specification for the Design of Cold-Formed Steel Structural Members, 2007 edition, American Iron and Steel Institute.
- [10] M. Sharp, B. Badders, M. Janssens, Modeling the Performance of Non-Loadbearing Gypsum-Protected Steel-Stud Walls in Furnace and Room Fire Tests, in: Proceedings of the 5th International Conference, Structures in Fire, Singapore, 2008, pp. 313–323.
- [11] R.J. Bryant, E.L. Johnsson, A. Hamins, B.S. Grove, W.F. Guthrie, A. Maranghides, G.W. Mulholland, NIST 3 Megawatt Quantitative Heat Release Rate Facility, NIST SP 1007, December 2003.
- [12] B.H. Jones, Performance of Gypsum Plasterboard Assemblies Exposed to Real Building Fires, M.S. Thesis, University of Canterbury, 2001.
- [13] Test Method for Fire Resistance Tests of Building Construction and Materials, ASTM E119-00a, American Society for Testing and Materials.
- [14] Eurocode 1—Actions on Structures Part 1–2: General Actions—Actions on Structures Exposed to Fire, EC1-1-2/59, 2001.
- [15] J.F. Nyman, H.J.T. Gerlich, C. Wade, A. Buchanan, Predicting fire resistance performance of drywall construction exposed to parametric design fires—a review, *J. Fire Prot. Eng.* 18 (2008) 117–139.
- [16] F. Alfawakhiri, M.A. Sultan, D.H. MacKinnon, Fire resistance of loadbearing steel-stud walls protected with gypsum board—a review, *Fire Technol.* 35 (1999) 308–335.
- [17] M.A. Sultan, Incident heat flux measurements in floor and wall furnaces of different sizes, *Fire Mater.* 30 (2006) 383–296.
- [18] G. Rein, C. Abecassis, A. Amundarain, H. Bateau, A. Cowlard, A. Chan, W. Jahn, A. Jowsey, P. Reszka, T. Steinhaus, S. Welch, J.L. Torero, J. Stern-Gottfried, A. Coles, M. Lazaro, D. Alvear, J.A. Capote, N.L. Ryder, F. Mowrer, C. Lautenberger, S. Desanghere, D. Joyeux, S. Kumar, Round-Robin study of fire modelling blind-predictions using the Dalmarnock Fire Experiments, in: Proceedings of the 5th ISFEH Conference, Edinburgh, April 2007.
- [19] S. Welch, A. Jowsey, S. Deeny, R. Morgan, J.L. Torero, BRE large compartment fire tests—characterizing post-flashover fires for model validation, *Fire Saf. J.* 42 (2007) 548–567.
- [20] World Trade Center Building Performance Study: Data Collection, Preliminary Observation, and Recommendation—Appendix A: An Overview of Fire Protection in FEMA 403, Buildings, Federal Emergency Management Agency, May 2002.
- [21] S.H. Park, S.L. Manzello, D.P. Bentz, T. Mizukami, Determining thermal properties of gypsum board at elevated temperatures, *Fire Mater.* 34 (2010) 237–250.
- [22] N. Bénichou, M. Sultan, Thermal properties of lightweight-framed construction components at elevated temperatures, *Fire Mater.* 29 (2005) 165–179.